Progress In Electromagnetics Research C, Vol. 79, 17–29, 2017

Optimization of Micromachined Millimeter-Wave Planar Silicon Lens Antennas with Concentric and Shifted Matching Regions

Henrik Frid*, Fritzi Töpfer, Shreyasi Bhowmik, Sergey Dudorov, and Joachim Oberhammer

Abstract—This paper presents a study of planar silicon lens antennas with up to three stepped-impedance matching regions. The effective permittivity of the matching regions is tailor-made by etching periodic holes in the silicon substrate. The optimal thickness and permittivity of the matching regions were determined by numerical optimization to obtain the maximum wideband aperture efficiency and smallest side-lobes. We introduce a new geometry for the matching regions, referred to as shifted matching regions. The simulation results indicate that using three shifted matching regions results in twice as large aperture efficiency as compared to using three conventional concentric matching regions. By increasing the number of matching regions from one to three, the band-averaged gain is increased by 0.3 dB when using concentric matching regions, and by 3.7 dB when using shifted matching regions, which illustrates the advantage of the proposed shifted matching region design.

1. INTRODUCTION

There is a growing interest in low-loss millimeter-wave antennas with fan-beam radiation patterns for communication [1] and radar [2]. Recently, several papers have presented the design, analysis and measurements of planar lens antennas with fan-beam radiation patterns for millimeter-wave frequencies [2–6]. The reported lens antennas have many advantages, including large bandwidths [3], frequency-stable far-fields, beam scanning capabilities [2, 6, 7] and frequency-stable phase center [3]. Planar lenses have many similarities with non-planar lenses, where there are many good references, see e.g., [8–13]. High-resistivity silicon is an excellent dielectric material for millimeter-wave planar lenses, due to its very small losses and accurate micromaching fabrication processes [14, 15]. However, homogeneous lenses of high permittivity materials, such as silicon, suffer from reflections at the air-dielectric interface caused by the large difference in impedance compared to free-space (see e.g., [9]). To reduce such reflections, high-permittivity lenses are commonly designed with up to three $\lambda/4$-matching regions, i.e., regions with permittivity and thickness determined as single or multiple $\lambda/4$-transformers [3, 9–11]. The advantages in using up to three $\lambda/4$-matching regions for non-planar rotationally symmetric lenses have been described in [11], based on time-domain simulations. The advantages described in [11] include improved forward-to-backward ratio and reduction of the beam distortions due to ground plane and substrate truncation.

A micromachined, planar extended hemispherical silicon lens prototype with a single matching region designed for W-band (75–110 GHz) was previously presented by the authors at a conference [16], see Fig. 1. The effective permittivity in the matching region was tailor-made by etching periodic holes in the silicon wafer, as described below in Section 2. One of the advantages of this antenna is the small size in the H-plane. It is therefore possible to use multiple planar lenses in a linear phased H-plane array.

Received 21 August 2017, Accepted 7 October 2017, Scheduled 17 October 2017
* Corresponding author: Henrik Frid (henrik.frid@ee.kth.se).
The authors are with the Micro and Nano Systems Laboratory, KTH Royal Institute of Technology, Stockholm, Sweden.

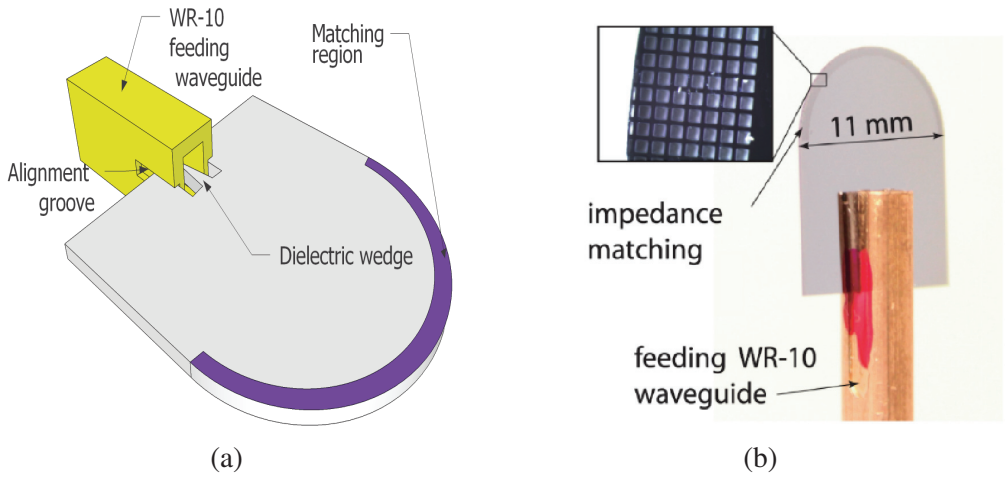

Figure 1. (a) Illustration of a planar silicon lens fed by a rectangular waveguide through a dielectric wedge transition. (b) Photograph of a fabricated W-band prototype antenna with a single matching region [16]. The period of the etch hole pattern in (b) is $p = 80\,\mu\text{m}$ and size of the square holes is $h = 60\,\mu\text{m}$, to obtain the effective relative permittivity of 4, as shown in Fig. 3.

Compared to conventional linear H-plane arrays of open-ended waveguides, an array of waveguide-mounted planar lenses has the advantage of higher gain and narrower beam in the E-plane. Such arrays usually have a relatively small scanning range, due to grating lobes appearing when scanning to large angles [17]. With appropriate care taken to avoid grating lobes, once could also consider this type of lens for sparse planar arrays and monopulse systems.

Interestingly, the optimal parameters for the matching region found in [16] were somewhat different compared to a $\lambda/4$-transformer. While [16] did not discuss the reason for the observed difference in thickness and permittivity compared to a $\lambda/4$-transformer, this can be explained due to the $\lambda/4$-transformer permittivity and thickness being derived for normal incidence [18], which is only satisfied approximately in a small area close to the center of the lens. The large variation in angle of incidence over a lens surface is shown in Fig. 2 in [13]. Based on this, it can be understood that $\lambda/4$-matching regions do not have the optimal thickness and permittivity to minimize the total internal reflections in lenses. The performance of lenses with matching regions could therefore potentially be improved by using an alternative method for determining the permittivity and thickness of the matching regions, or by using matching regions of different geometry. In this paper, we address the problem of finding optimal matching region thickness and permittivity for planar silicon lenses. Matching regions with thickness and permittivity different from the conventional $\lambda/4$-transformer have been studied for non-planar lenses [19, 20], and for radomes [21].

Previously reported lenses typically use matching regions of uniform thickness [3, 9–11], here referred to as concentric matching regions. In this paper, we present a new matching region geometry, referred to as a shifted matching region. This new geometry was inspired by studying the simplified problem of oblique incidence on a single matching region on a semi-infinite dielectric slab, see e.g., [18]. The impedance of the matching region is described by a parallel impedance (for TM polarization) and a transverse impedance (for TE polarization), which depend differently on the angle of incidence depending on the polarization. Following [18], it is possible to calculate the permittivity and thickness of the matching region, which eliminates the reflection for a single angle of incidence, frequency and polarization. This simplified example illustrates the difficulties in designing matching regions, since the reflection coefficient depends on frequency, polarization and angle of incidence. Interestingly, the matching region thickness which eliminates the reflection at a single frequency, increases with increasing angle of incidence for TE polarization, but decreases for TM polarization. This observation is the basis for the here proposed shifted matching region.

Compared to [16], which considered only a single matching region of concentric type, this paper presents an analysis of planar silicon lenses with up to three matching regions. Furthermore, while [16] focuses on microfabrication and measurements, this paper presents a numerical optimization approach to

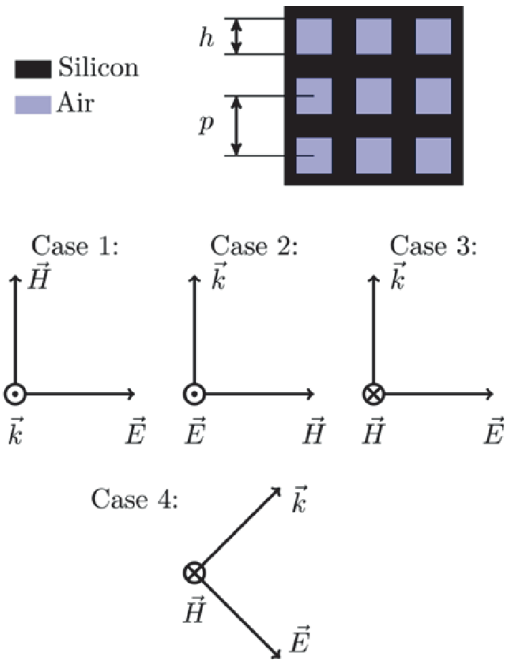

Figure 2. Illustration of a silicon wafer with square holes of size h and period p. The investigated cases of TEM polarization have been marked in the figure. Case 4 is related to Case 3 by a 45° rotation around the H-axis.

determine optimal matching regions. The measurement results for the prototype were in good agreement with simulations [16]. For sake of brevity, the measurement results from [16] are not repeated here, and the reader is instead referred to [16]. In Section 3.1, we discuss the choice of cost function to use in the optimization. Numerical results are presented in Sections 3.2 and 3.3. Finally, conclusions are drawn in Section 4.

2. TAILOR-MADE EFFECTIVE PERMITTIVITY REGIONS IN A SILICON WAFER

The method of artificially lowering the permittivity of a dielectric material by introducing a density of spherical or cylindrical holes was demonstrated already in the 1950s [22]. This type of artificial dielectrics have since then been used in antenna design (e.g., [2, 7]), for test samples with a known permittivity [14], and in the design of W-band phase shifters [23]. We here use this technique in order to achieve tailor-made permittivities for the matching regions in the proposed lens antennas by etching periodic square holes of width h and period p in a silicon wafer according to Fig. 2. The period p was chosen to be 80 µm, which is significantly smaller than the wavelength λ_d at W-band (75–110 GHz). This period was chosen since it is very well suited for deep reactive ion etching (DRIE) with straight side-walls in silicon. Since $\lambda_d \gg p$, the effective relative permittivity ϵ_{eff} is to a good approximation independent of the frequency, and it can be calculated in the long-wave limit [22]. It is interesting to note that the polarizability of cylinders (which are here implemented with a square cross-section) depends on the direction of the applied electric field, and the effective permittivity will therefore not be the same for all the cases of plane wave propagation depicted in Fig. 2. Thus, the effective material is anisotropic such that Cases 1, 3 and 4, for which the applied electric field is perpendicular to the cylindrical air holes, correspond to the perpendicular permittivity component $\epsilon_\perp$, whereas Case 2 corresponds to the parallel component $\epsilon_\parallel$. Due to the polarization of the TE_{10} mode in the feeding waveguide in Fig. 1, the propagation through the matching regions of the proposed antenna is described by Cases 3 and 4 illustrated in Fig. 2. Following [7], the effective relative permittivity is calculated according to:

$$\epsilon_{eff} = \epsilon_s \frac{\epsilon_s(1-\kappa)+\kappa+K_d(1-(\epsilon_s(1-\kappa)+\kappa))}{\epsilon_s+K_d(1-(\epsilon_s(1-\kappa)+\kappa))}, \tag{1}$$

where $\kappa = (h/p)^2$ is the volume density of holes, and $\epsilon_s = 11.6$ is the relative permittivity of the surrounding high-resistivity silicon substrate. The depolarization coefficient, K_d, equals 0.5 if the electric field vector is perpendicular to the hole axis (cases 1, 3, 4) and 0 if the electric field vector is parallel to the hole axis (case 2), whereby both $\epsilon_\perp$ and $\epsilon_\parallel$ can be calculated using Eq. (1). In order to verify the validity of Eq. (1), in addition to determining the frequency-dependence of ϵ_{eff} not given by Eq. (1), the effective relative permittivity was derived from numerical simulation for the four cases of plane wave propagation depicted in Fig. 2. We determine ϵ_{eff} directly from the dispersion diagram, which is calculated using eigenmode analysis of the unit cell. The Eigenmode Solver implemented in [24] was used for this simulation. Since the relative permeability of silicon is very close to 1 in the W-band [15], we have $n = \sqrt{\epsilon_{eff}}$ where n is the calculated refractive index. Based on the simulated dispersion relation (i.e., the relation between the wave number k and the angular frequency ω), the permittivity was extracted according to $\epsilon_{eff} = (ck/\omega)^2$ where c is the speed of light in vacuum. The numerical results are presented in Fig. 3(a), in excellent agreement with (1). The permittivity is also presented as a function of frequency in Fig. 3(b). The standard deviation in the calculated relative permittivity is smaller than 0.012 for all curves in Fig. 3(b), which demonstrates that the effective material is independent of the frequency to a very good approximation in the W-band. Hence, we conclude that 80 µm is a sufficiently small hole period for achieving a frequency-independent permittivity. It can also be seen in Fig. 3 that the material is only weakly anisotropic. It is also possible to calculate ϵ_{eff} from simulated reflection or transmission coefficients for TEM waves incident on a semi-infinite slab of the considered material, see e.g., [25].

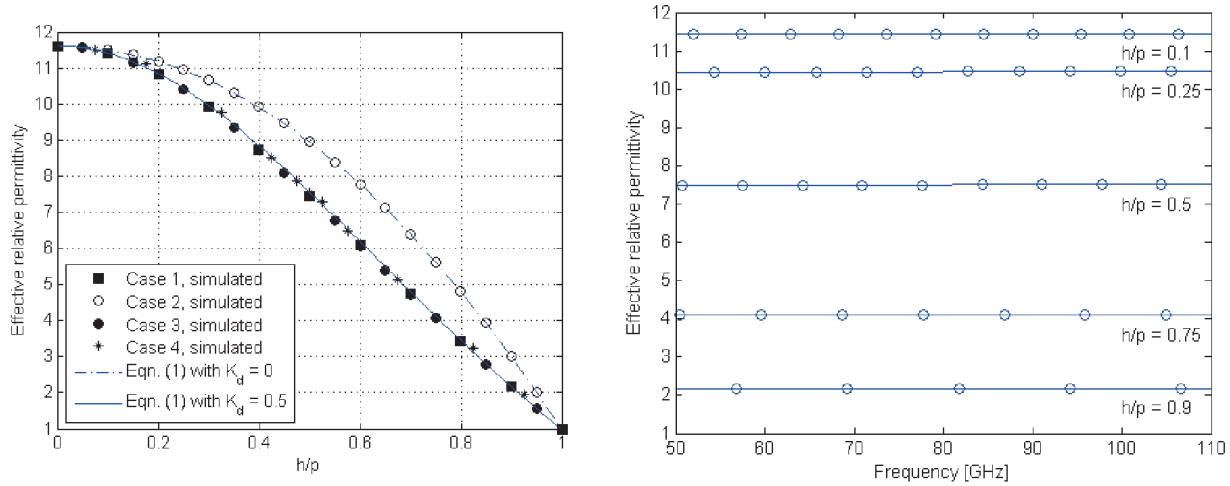

(a) (b)

Figure 3. (a) Effective relative permittivity of a silicon substrate with periodic square holes of size h and period $p = 80\,\mu\text{m}$, derived from simulation, as a function of the normalized hole size h/p. The agreement with the theoretical curve (1) is excellent. (b) Effective relative permittivity for Case 3 extracted as a function of frequency from the simulated dispersion diagram.

3. MATCHING REGION CONCEPTS FOR PLANAR SILICON LENSES

3.1. Overview

In this section, we present a comparison between different matching region concepts for planar extended hemispherical lenses of diameter D, as illustrated in Fig. 4. We also present the optimization method used to determine optimal values of the thickness and permittivity of each matching region. Since the antenna gain G is related to the physical aperture area A_p according to $G = 4\pi e_a A_p/\lambda^2$ [18], where e_a is the aperture efficiency, it is important to consider the same physical aperture size when comparing the different matching region concepts. The matching regions are therefore implemented such that the diameter D is the same for all investigated designs, independently of the thickness of the matching

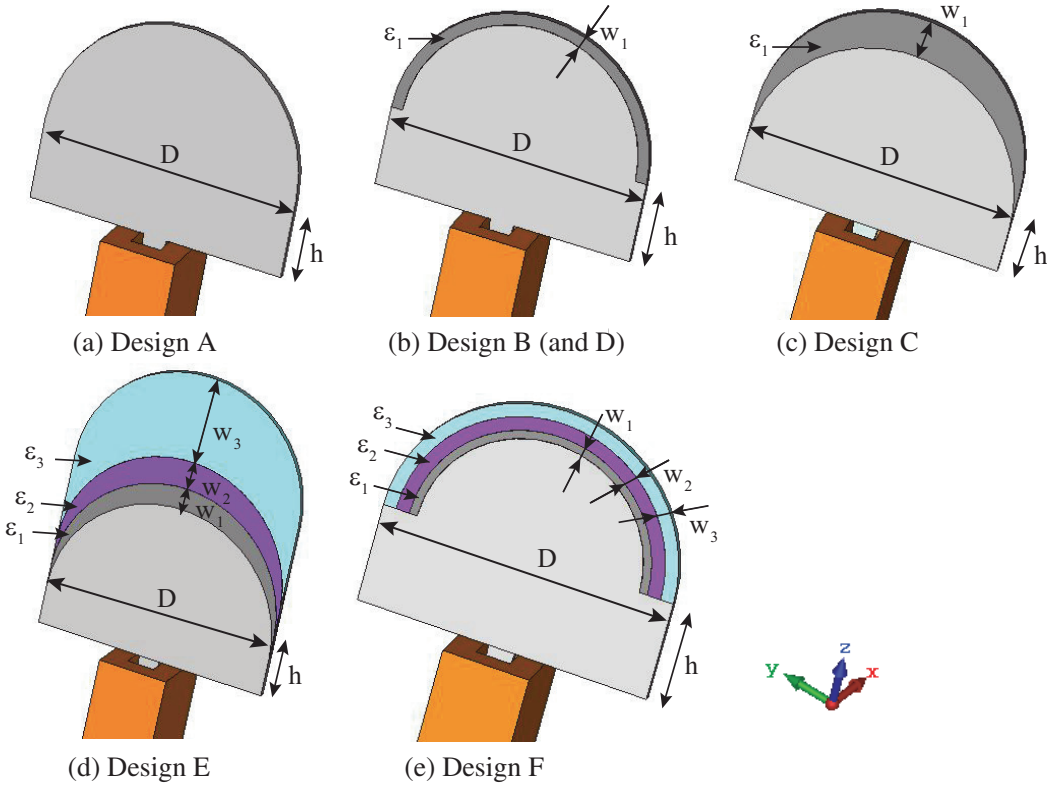

Figure 4. Different implementations of matching regions for planar extended hemispherical silicon lenses: (a) Design A: no matching region, (b) Design B: single concentric matching region, (c) Design C: single shifted matching region, (d) Design E: three shifted matching regions and (e) Design F: three concentric matching regions. The relevant parameters for matching region i are the relative permittivity ϵ_i and the width w_i. Design D is based on Design B with ϵ_1 and w_1 calculated as a $\lambda/4$-transformer at 100 GHz.

regions. Thus, we investigate which matching region concept in Fig. 4 results in the highest gain for the same physical aperture size, i.e., we are interested in determining which design results in the highest aperture efficiency. A 300 µm thick high-resistivity ($\tan\delta = 6{\cdot}10^{-4}$) silicon wafer is considered for lenses of diameter $D = 11$ mm for this study, in order to compare with the measured prototype from [16]. The free-etched lenses are installed on a WR-10 waveguide. The tapered dielectric wedge transition was designed following [14], and minimizes reflections at the boundary between the feeding waveguide and the dielectric body of the lens throughout the W-band (75–110 GHz).

The simplest design without any matching region is referred to as Design A. By including a single matching region, as illustrated for Designs B-C in Fig. 4, it is possible to reduce the reflections at the boundary between the lens and free-space. Design B has a single concentric matching region, just like prototype in [16], while Design C has a single shifted matching region. This shifted matching region is defined as the difference between two circles with the same diameter, where one is shifted (translated) by a distance w_1 along the direction of the waveguide, with respect to the other. The motivation of this novel matching region geometry is described below. As described in Section 1, we do not expect a matching region with thickness and permittivity determined as a $\lambda/4$-transformer to provide the optimal matching region. For sake of comparison, we therefore define Design D based on Design B, with ϵ_1 and w_1 calculated as a $\lambda/4$-transformer at 100 GHz.

For the lenses presented in Fig. 1 and Fig. 4, the wave launched through the dielectric wedge into the dielectric slab is TM-polarized with respect to the lens surface. From the simplified case of a plane wave incident on a semi-infinite slab with a single matching region described above and in [18], we know that the thickness which eliminates the reflection at a single frequency, decreases with increasing angle for TM polarization. Therefore, it seems that the best matching region would not be uniform

as the concentric geometry (Designs B and F), but rather be tapered to be thinner at larger angles of incidence, towards the edges of the lens. Although there are several geometries of tapering the thickness, we have for sake of simplicity used a shifted geometry (Designs C and E), as described above. From transmission-line theory, it can be expected that using multiple matching regions will improve the performance compared to using a single matching region [18, 26]. Three matching regions were used for Designs E and F.

The optimal parameters for each design considered in Fig. 4 have been determined using Trust Region Framework (TRF) optimization together with the Finite Integration Technique (FIT) implemented in [24]. Firstly, we attempted to minimize the return loss in the entire W-band (Objective I). Secondly, we attempted maximizing the averaged gain over this frequency band (Objective II). Thirdly, we attempted maximizing the band-averaged gain while simultaneously minimizing the side-lobe level with equal weights of the goals (Objective III). It is interesting to note that all three choices of objective functions resulted in similar parameters and antenna performance. All objectives resulted in similar band-averaged gain, the only difference being, Objective III resulted in the smallest side-lobe level, about 2 dB lower than obtained using Objectives I or II. Therefore, the results from the optimization using Objective III are presented here. Section 3.2 presents the comparison between Designs A-D which are based on a single matching region, and Section 3.3 presents the comparison between Designs E-F, which are based on three matching regions. The optimized parameters are presented in Table 1, and the band-averaged figures-of-merit for each design are summarized in Table 2. Once the optimal permittivity is obtained, the corresponding hole size h to be used for fabrication is readily extracted from Fig. 3. Since the optimization problem is not convex, special care needs to be taken in order to ensure that the optimal value determined using TRF optimization is not only a local minimum, but a global minimum. We therefore repeated the TRF optimization several times using several different initial values. Thus, we believe that the parameter set presented in Table 1 corresponds to the global optimum.

Table 1. Design parameters, determined using TRF optimization, for Designs A-F, as defined in Fig. 4. For sake of comparing the aperture efficiency, all designs have the same diameter, $D = 11$ mm.

	Extension Height, h (mm)	Relative permittivity, ϵ_i	Width, w_i (mm)
Design A	3.4	-	-
Design B	3.4	6.4	0.48
Design C	1.8	9.7	1.54
Design D	3.4	3.4	0.41
Design E	1.74	7.73, 4.92, 2.73	1.43, 2.49, 4.18
Design F	3.55	10.5, 8.33, 4.12	0.27, 0.49, 0.51
Prototype [16]	3.0	4.0	0.50

Table 2. Calculated figures-of-merit for Designs A-F presented in Fig. 4. These figures-of-merit were calculated as an average over the W-band (75–110 GHz). As usual, the notation S_{11} is used for the reflection coefficient, and side-lobe level is abbreviated by SLL.

	Gain (dB)	S_{11} (dB)	E-plane SLL (dB)	H-plane SLL (dB)	Cross-pol. (dB)
Design A	12.5	−15.3	−9.72	−12.2	−12.5
Design B	13.7	−21.3	−16.1	−14.4	−17.5
Design C	13.3	−17.8	−13.8	−10.6	−15.2
Design D	13.2	−17.7	−14.1	−11.5	−15.8
Design E	17.4	−19.3	−14.7	−18.7	−22.8
Design F	14.0	−20.8	−14.2	−17.1	−17.4
Prototype	13.1	−19.1	−13.1	−14.1	−15.1

It is expected that the accuracy of the simulation results compared to measurements is mainly determined by fabrication tolerances in the silicon microfabrication process, in addition to the accuracy when installing the lens on the feeding waveguide. The fabrication and measurements are beyond the scope of this paper, and the reader is instead referred to [16].

As can be seen in Fig. 4, Design E is longer in the z-direction than Design F. Note that the aperture area A_p is defined in the xy-plane [18], whereby the length in the z-direction does not affect the physical aperture area. Meanwhile, it is interesting to note that Design E has a larger focal length than Design F, thereby occupying a larger volume. It is typical that quasi-optical systems become more efficient as they increase in length, however only until a certain threshold value. Beyond that, the gain can only be increased by increasing the diameter [18]. The same phenomenon is seen in array antenna elements such as the BoR-element [27], which also becomes more efficient when made longer, but it is ultimately limited by the area occupied in the xy-plane. In addition to the above, it is also important to compare the available gain for a fixed diameter when considering sparse arrays consisting of multiple lenses. In a planar array, each element has only a fixed area in the xy-plane. For some applications such as sparse arrays and monopulse systems, it is needed to maximize the gain produced using this fixed area. For such applications, the length is not a critical parameter, unless it results in a significantly increased weight. Thus, the diameter (or equivalently, the area in the xy-plane) becomes the most important limitation. Based on the above, we have decided to compare the lenses for a fixed diameter, but without limitation on the length.

3.2. Wideband Analysis of Planar Lenses with a Single Matching Region

Starting with Design A, the extension height h was determined to maximize the gain. The same extension height was used for Designs B, C and D. The thickness and permittivity for Designs B and C were determined using TRF optimization, with Objective III described above. The design parameters for all designs are presented in Table 1. Hence, Designs B and C were optimized for two parameters (w_1 and ϵ_1), and there was no significant change in the optimal parameters when optimizing for three parameters (i.e., w_1, ϵ_1 and h). Note that there is some difference in optimal parameters for Design B compared to the prototype in [16]. This is due to different optimization goals used here compared to [16]. The reflection coefficient is presented as a function of frequency in Fig. 5, while the gain, side-lobe level and cross-polarization are presented as functions of frequency in Fig. 6. Band-averaged figures-of-merit are presented in Table 2.

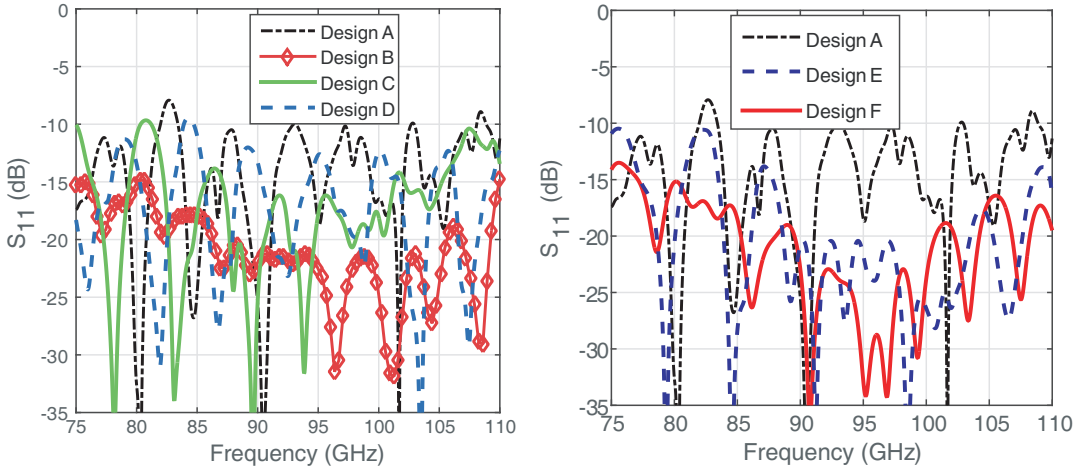

Figure 5. Calculated reflection coefficient for (a) lenses with a single matching region (Designs B-D) and (b) lenses with three matching regions (Designs E-F). Compared to a lens without any matching region (Design A), the introduction of (a) single matching regions and (b) three matching regions, substantially reduces the return loss. It can also be seen that the return loss is reduced in a wideband sense over the entire frequency band.

Firstly, we consider the reflection coefficients in Fig. 5(a). While the $\lambda/4$-transformer used for Design D is designed for 100 GHz, we note that Design D improves the return loss, as compared to Design A, not only at 100 GHz, but also on average over the entire W-band. The reflection coefficient varies rapidly with frequency for all designs (see Fig. 5), but due to the optimized dielectric wedge transition (Fig. 1), the maximum return loss is relatively small even for Design A, which at worst has 8 dB return loss within the band.

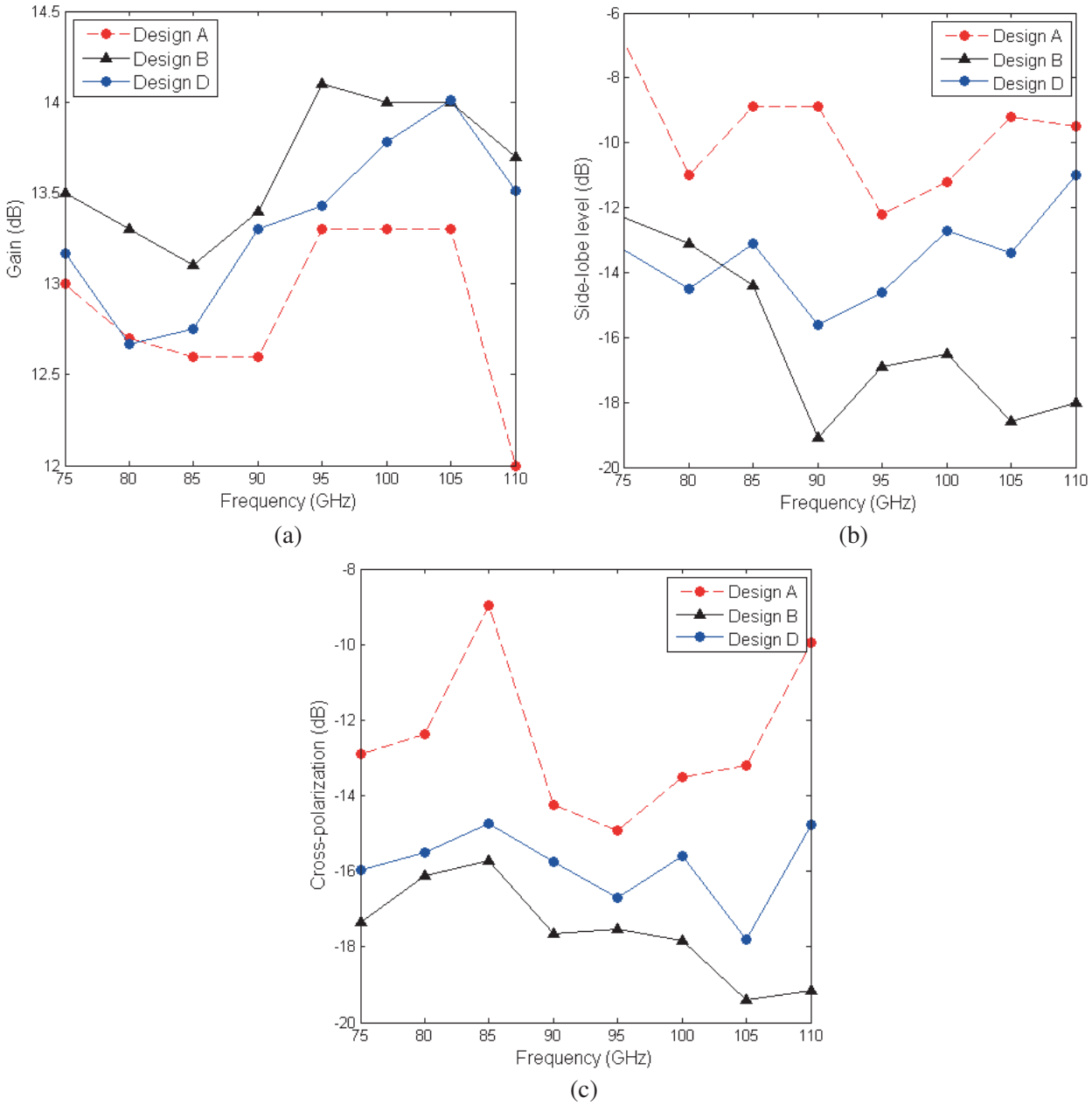

Figure 6. Calculated (a) gain (b) side-lobe level and (c) cross-polarization for Designs A, B and D as a function of frequency. Design A has no matching region, Design D has a $\lambda/4$-transformer matching, and Design B has an optimized matching region. By reduction of internal reflections, both Designs B and D have higher gain, lower side-lobe level and smaller cross-polarization than Design A. It is also seen that the optimized matching region for Design B is superior to the commonly used $\lambda/4$-transformer (Design D).

The inclusion of the $\lambda/4$-transformer in Design D increases the gain while reducing the side-lobe level and the cross-polarization, see Fig. 6. While Design D is an improvement as compared to Design A, it is possible to improve the performance further by using an optimized matching region. Design B has smaller return loss (Fig. 5(a)), higher gain (Fig. 6(a)), smaller side-lobe level (Fig. 6(b)) and smaller cross-polarization (Fig. 6(c)) than Design D. As can be seen in Table 1, the optimal values for Design B are also somewhat different that for Design D. Hence, we have found that the conventional $\lambda/4$-transformer (Design D) does not provide the optimal parameters for the matching region for small planar lenses ($D = 11\,\text{mm}$). In conclusion, Table 2 shows that Design B has the highest gain (and consequently also the highest aperture efficiency), lowest side-lobe level, cross-polarization and return loss, all of which are superior to Designs A, C and D. While Design C does not provide an improvement compared to Design B, the advantages in using the shifted matching region from Design C will become demonstrated in the following section where we consider multiple matching regions.

3.3. Wideband Analysis of Planar Lenses with Three Matching Regions

In total, 7 parameters were determined for Designs E and F, i.e., the extension height, in addition to the thickness and permittivity of all three matching regions. As a starting point for the optimization, we used multistage $\lambda/4$-transformer matching regions, see e.g., [26]. The optimized permittivity and width for each matching region is presented in Table 1. As seen in Table 2, the band-averaged gain of the optimized lens is 17.4 dB for Design E, and 14.0 dB for Design F. Compared to Design B, which is the best design with a single matching region, with band-averaged gain of 13.7 dB, there is only a small improvement in increasing the number of concentric matching regions. Meanwhile, there was a 3.7 dB increase in the band-averaged gain when using three shifted matching regions. A comparison between the far-field radiation patterns of Designs E and F is found in Fig. 7. It is interesting to consider the frequency 100 GHz, where Design E has more than 3 dB higher gain than Design F, whereby the effective area of Design E is at least twice as large as for Design F. Thus, we can conclude that, while maintaining the same physical aperture size, Design E proves to be superior to Design F in terms of its aperture efficient design. Fig. 7 shows that there are relatively small variations over frequency. The wideband performance is therefore well captured by the average values presented in Table 2. In addition to the highest band-averaged gain, Design E also has the lowest band-averaged cross-polarization, which is 5 dB lower than Designs B and F, see Table 2.

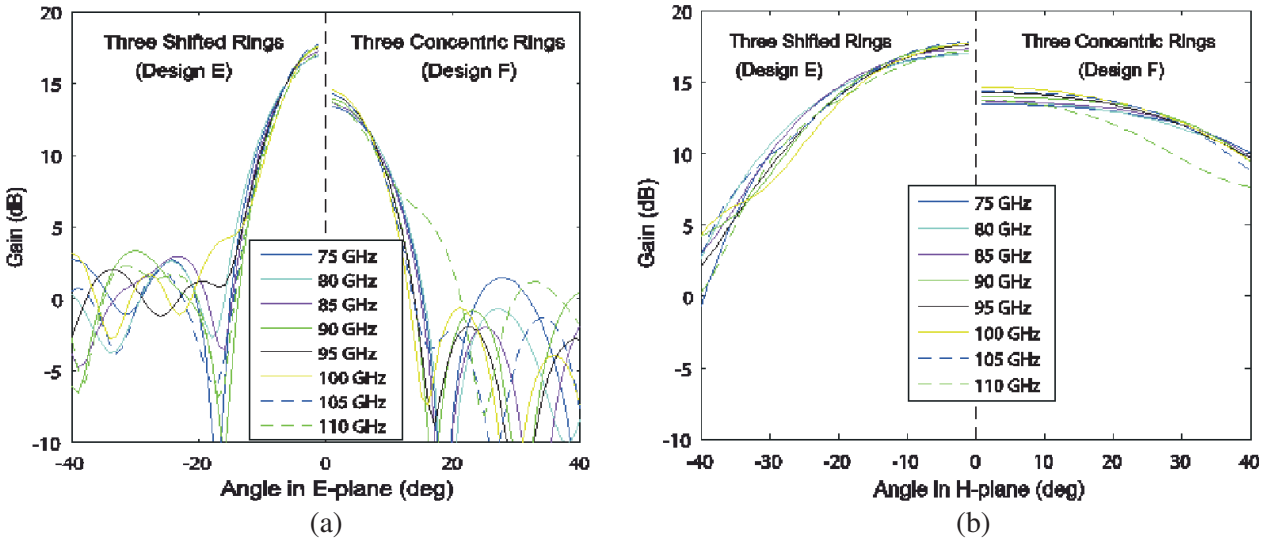

Figure 7. Calculated gain in (a) E-plane and (b) H-plane for Design E and Design F. The far-field pattern has the shape of a fan-beam, with a wide beam in the H-plane and a narrow beam in the E-plane.

Figure 8 presents near-field plots for Designs A and E, in both E- and H-planes. This figure shows how the lens acts as a matching from the TE_{10} mode, to free-space TEM waves. It can be seen that the antenna radiates with a flat phase front (and consequently a narrow beam) in the E-plane, and a wide beam in the H-plane. This explains the fan-beam shape of the far-field pattern seen in Fig. 7. The internal reflections for Design A are clearly visible in Fig. 8(b), which has a severely disturbed field with a clearly visible standing waves within the lens, which is greatly improved for Design E in Fig. 8(d). Fig. 8(b) also shows that there are some back-lobes forming for Design A. Considering Table 2, we note that the internal reflections increase the amount of power radiated into the side-lobes, and increase the cross-polarization, thus decreasing the gain. Another interesting observation in the H-plane near-field plot for Design E (Fig. 8(c)) is the concentration of the electric field to the high-permittivity silicon slab. This is similar to the field concentration seen in dielectric rod waveguides [14], where the field concentration is more significant for larger permittivity values. Since Design E has a permittivity which decreases in three steps, over the relatively long matching regions, we note that the field widens around the lens as it propagates through the regions of lower permittivity. This effect is clearly visible in Fig. 8(c).

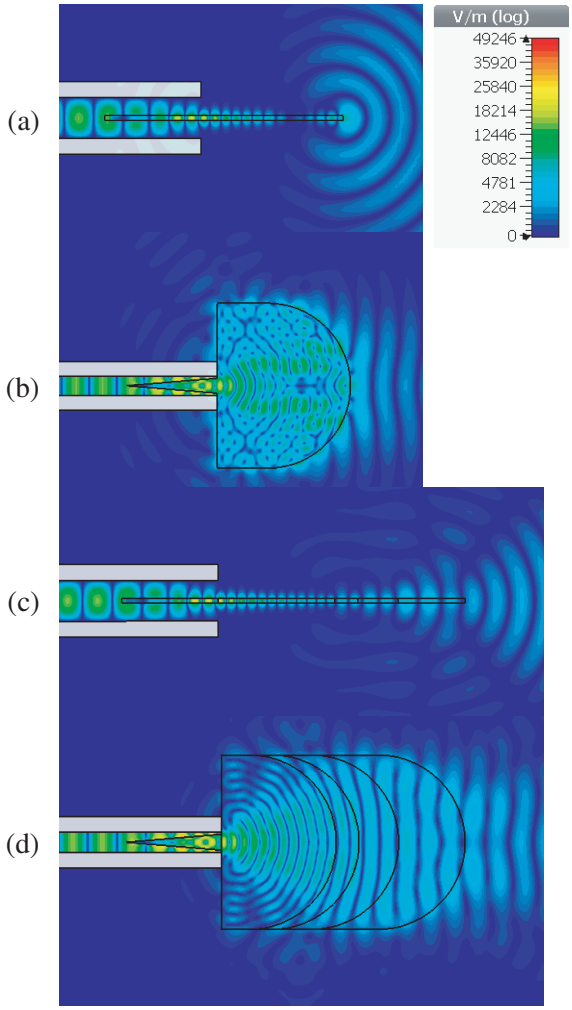

Figure 8. Logarithmic near-field plot of the electric field magnitude at 100 GHz, demonstrating the transition from the waveguide TE_{10} mode to free-space TEM waves, for (a)–(b) Design A and (c)–(d) Design E, in H- and E-planes. The internal reflections for Design A are clearly visible in (b). There is a flat phase front in the E-plane, see (b) and (d), and a wide beam in the H-plane, see (a) and (c), which results in a fan-beam radiation pattern.

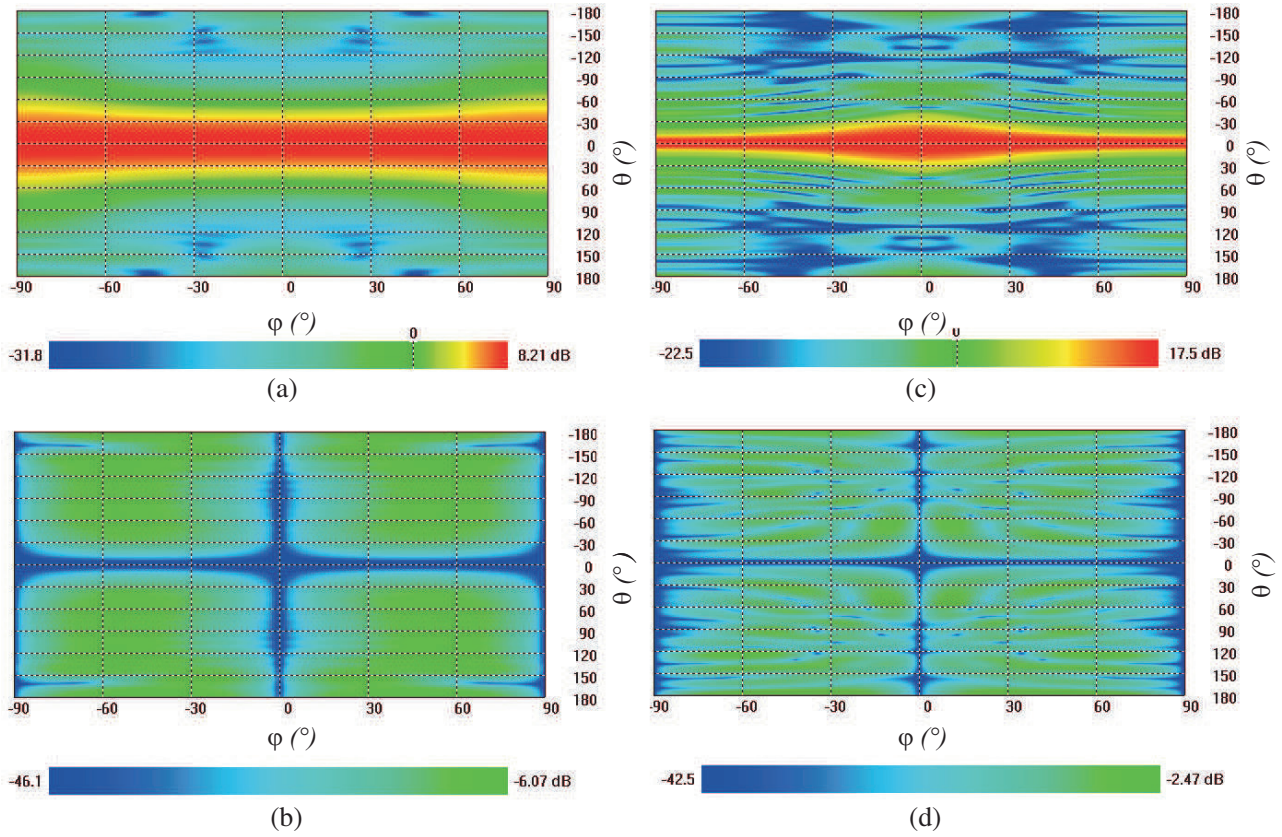

Figure 9. Calculated realized gain at 100 GHz for (a) co-polarization open-ended waveguide, (b) cross-polarization for open-ended waveguide, (c) co-polarization for Design E and (d) cross-polarization for Design E. The cross-polarization is zero in principal planes both for the open-ended waveguide and the lens antenna. Note that the sub-figures are arranged with the open-ended waveguide results to the left and the corresponding lens results to the right.

The cross-polarization values presented in Table 2 are calculated as the maximum cross-polarization (evaluated over all angles), normalized by the co-polarization in the main lobe (i.e., $\theta = 0°$), based on Ludwig's 3rd definition [28]. The angular dependence of the cross-polarization is similar to that of an open-ended waveguide, with zeros in the principal planes ($\phi = 0°, \pm 90°$) due to symmetry [29], and the maximum value occurring roughly at 45° between the two planes, see Fig. 9. Based on the above, the cross-polarization values presented in Table 2 represent a worst-case estimate averaged over the frequency band.

4. CONCLUSIONS

This paper presents the design and optimization of planar silicon-micromachined extended hemispherical lens antennas, with up to three stepped-impedance matching regions. The primary aim of this paper is to describe how to obtain optimal matching regions for this type of lens. The width and permittivity of each matching region was determined using TRF optimization. The optimization cost function was chosen to maximize the gain while simultaneously minimizing the side-lobe level over a wide frequency range (75–110 GHz), as described in Section 3.1. It has been demonstrated that the introduction of matching regions result in a wideband improvement of return loss, side-lobe level and cross-polarization, while increasing the aperture efficiency.

An important result is that the optimal width and permittivity of a single matching region, determined using optimization, differs from those of a $\lambda/4$-transformer. This can be explained by the fact that the derivation of the $\lambda/4$-transformer assumes normal incidence, which is only valid in a

small area in the center of the lens. This illustrates that the conventional $\lambda/4$-transformer matching region is not optimal for this type of lens. The optimized single matching region (Design B) provides an improvement compared to the conventional $\lambda/4$-transformer (Design D) since the width and permittivity are optimized to achieve the best performance, which allows the optimal trade-off to partly compensate for the geometry of the lens and matching region.

When considering oblique TM incidence on a semi-infinite dielectric slab with a single matching region, the thickness of the matching region should be slightly smaller than $\lambda/4$ [18]. This is the reason why the proposed shifted matching region is tapered such that the thickness decreases towards the edges, where the angle of incidence is greater. The presented simulation results indicate that the matching region geometry is an important parameter which can be varied to improve the performance. The simplicity of the shifted matching regions used here could explain why Design C does not provide an improvement compared to Design B. Meanwhile, we noted a significant improvement when comparing three concentric matching regions (Design F) with three shifted matching regions (Design E). From the simulation results, it can be concluded that increasing the number of concentric matching regions does not result in a significant improvement compared to using a single concentric matching region. However, by using three shifted matching regions, it was possible to increase the gain significantly, while the aperture size remained the same. Thus, we conclude that the proposed shifted matching region geometry is superior to the concentric geometry when three matching regions are used.

It is an interesting observation that the stepped matching regions we have considered here could be thought of as discretization of the permittivity distribution in a gradient-index (GRIN) lens (see e.g., [30–32]). Similarly to most GRIN-lenses, the permittivity distribution in Design E and F presented here is monotonically decreasing from the maximum value, as we move closer to the air-dielectric interface. Since Design E is superior to Design F, we make the interpretation that the shifted region is more efficient than the concentric region for discretizing a planar hemispherical GRIN lens. Furthermore, the silicon-micromachining process used here is not limited to stepped-permittivity matching regions, whereby this fabrication process is of interest for future planar silicon-GRIN lenses.

REFERENCES

1. George, J., P. F. M. Smulders, and M. H. A. J. Herben, "Application of fan-beam antennas for 60 GHz indoor wireless communication," *Electronics Letters*, Vol. 37, No. 2, 73–74, Jan. 2001.
2. Xue, L. and V. Fusco, "24 GHz automotive radar planar Luneburg lens," *IET Microwaves, Antennas & Propagation*, Vol. 1, No. 3, 624–628, 2007.
3. Tokan, F., N. T. Tokan, A. Neto, and D. Cavallo, "The lateral wave antenna," *IEEE Transactions on Antennas and Propagation*, Vol. 62, No. 6, 2909–2916, 2014.
4. Xue, L. and V. Fusco, "Polarisation insensitive planar dielectric slab waveguide extended hemielliptical lens," *IET Microwaves, Antennas & Propagation*, Vol. 2, No. 4, 312–315, 2008.
5. Rolland, A., R. Sauleau, and L. Le Coq, "Flat-shaped dielectric lens antenna for 60-GHz applications," *IEEE Transactions on Antennas and Propagation*, Vol. 59, No. 11, 4041–4048, 2011.
6. Xue, L. and V. Fusco, "Patch fed planar dielectric slab extended hemi-elliptical lens antenna," *IEEE Transactions on Antennas and Propagation*, Vol. 56, No. 3, 661–666, 2008.
7. Sato, K. and H. Ujiie, "A plate luneberg lens with the permittivity distribution controlled by hole density," *Electronics and Communications in Japan (Part I: Communications)*, Vol. 85, No. 9, 1–12, 2002.
8. Karttunen, A., J. Saily, A. E. Lamminen, J. Ala-Laurinaho, R. Sauleau, and A. V. Raisanen, "Using optimized eccentricity rexolite lens for electrical beam steering with integrated aperture coupled patch array," *Progress In Electromagnetics Research B*, Vol. 44, 345–365, 2012.
9. Filipovic, D. F., S. S. Gearhart, and G. M. Rebeiz, "Double-slot antennas on extended hemispherical and elliptical silicon dielectric lenses," *IEEE Transactions on Microwave Theory and Techniques*, Vol. 41, No. 10, 1738–1749, 1993.
10. Neto, A., "UWB, non dispersive radiation from the planarly fed leaky lens antenna. Part 1: Theory and design," *IEEE Transactions on Antennas and Propagation*, Vol. 58, No. 7, 2238–2247, 2010.
11. Nguyen, N. T., R. Sauleau, and C. J. M. Perez, "Very broadband extended hemispherical

lenses: Role of matching layers for bandwidth enlargement," *IEEE Transactions on Antennas and Propagation*, Vol. 57, No. 7, 1907–1913, 2009.

12. Fernandes, C. A., E. B. Lima, and J. R. Costa, "Broadband integrated lens for illuminating reflector antenna with constant aperture efficiency," *IEEE Transactions on Antennas and Propagation*, Vol. 58, No. 12, 3805–3813, 2010.
13. Frid, H., "Closed-form relation between the scan angle and feed position for extended hemispherical lenses based on ray tracing," *IEEE Antennas and Wireless Propagation Letters*, Vol. 15, 1963–1966, 2016.
14. Töpfer, F., S. Dudorov, and J. Oberhammer, "Millimeter-wave near-field probe designed for high-resolution skin cancer diagnosis," *IEEE Transactions on Microwave Theory and Techniques*, Vol. 63, No. 6, 2050–2059, 2015.
15. Sterner, M., N. Somjit, U. Shah, S. Dudorov, D. Chicherin, A. Räisänen, and J. Oberhammer, "Microwave MEMS devices designed for process robustness and operational reliability," *International Journal of Microwave and Wireless Technologies*, Vol. 3, No. 5, 547–563, 2011.
16. Dudorov, S., F. Töpfer, and J. Oberhammer, "Micromachined-silicon W-band planar-lens antenna with metamaterial free-space matching," *2012 IEEE MTT-S International Microwave Symposium Digest (MTT)*, 1–3, IEEE, 2012.
17. Mailloux, R. J., *Phased Array Antenna Handbook*, Vol. 2, Artech House Boston, 2005.
18. Goldsmith, P. F., *Quasioptical Systems: Gaussian Beam Quasioptical Propagation and Applications*, IEEE Press New York, 1998.
19. Costa, J. R., C. A. Fernandes, G. Godi, R. Sauleau, L. Le Coq, and H. Legay, "Compact Ka-band lens antennas for leo satellites," *IEEE Transactions on Antennas and Propagation*, Vol. 56, No. 5, 1251–1258, 2008.
20. Silveirinha, M. G. and C. A. Fernandes, "Shaped double-shell dielectric lenses for wireless millimeter wave communications," *IEEE Antennas and Propagation Society International Symposium*, Vol. 3, 1674–1677, IEEE, 2000.
21. Fitzek, F. and R. H. Rasshofer, "Automotive radome design-reflection reduction of stratified media," *IEEE Antennas and Wireless Propagation Letters*, Vol. 8, 1076–1079, 2009.
22. Ward, H., W. Puro, and D. Bowie, "Artificial dielectrics utilizing cylindrical and spherical voids," *Proceedings of the IRE*, Vol. 44, No. 2, 171–174, 1956.
23. Somjit, N., G. Stemme, and J. Oberhammer, "Binary-coded 4.25-bit w-band monocrystalline — Silicon mems multistage dielectric-block phase shifters," *IEEE Transactions on Microwave Theory and Techniques*, Vol. 57, No. 11, 2834–2840, 2009.
24. CST Microwave Studio, 2016, www.cst.com.
25. Liu, L., S. Matitsine, Y. Gan, and K. Rozanov, "Effective permittivity of planar composites with randomly or periodically distributed conducting fibers," *Journal of Applied Physics*, Vol. 98, No. 6, 063512, 2005.
26. Collin, R. E., *Foundations for Microwave Engineering*, John Wiley & Sons, 2007.
27. Holter, H., "Dual-polarized broadband array antenna with BOR-elements, mechanical design and measurements," *IEEE Transactions on Antennas and Propagation*, Vol. 55, No. 2, 305–312, 2007.
28. Ludwig, A., "The definition of cross polarization," *IEEE Transactions on Antennas and Propagation*, Vol. 21, No. 1, 116–119, 1973.
29. Silver, S., *Microwave Antenna Theory and Design*, No. 19, IET, 1949.
30. Jain, S., M. Abdel-Mageed, and R. Mittra, "Flat-lens design using field transformation and its comparison with those based on transformation optics and ray optics," *IEEE Antennas and Wireless Propagation Letters*, Vol. 12, 777–780, 2013.
31. Quevedo-Teruel, O., W. Tang, R. C. Mitchell-Thomas, A. Dyke, H. Dyke, L. Zhang, S. Haq, and Y. Hao, "Transformation optics for antennas: Why limit the bandwidth with metamaterials?" *Scientific Reports*, Vol. 3, 2013.
32. Mei, Z. L., J. Bai, and T. J. Cui, "Gradient index metamaterials realized by drilling hole arrays," *Journal of Physics D: Applied Physics*, Vol. 43, No. 5, 055404, 2010.